Page curve under final state projection

Ibrahim Akal,[1,*] Taishi Kawamoto,[1,†] Shan-Ming Ruan,[1,‡] Tadashi Takayanagi,[1,2,3,§] and Zixia Wei[1,‖]

[1]*Center for Gravitational Physics and Quantum Information, Yukawa Institute for Theoretical Physics, Kyoto University, Kitashirakawa Oiwakecho, Sakyo-ku, Kyoto 606-8502, Japan*

[2]*Inamori Research Institute for Science, 620 Suiginya-cho, Shimogyo-ku, Kyoto 600-8411, Japan*

[3]*Kavli Institute for the Physics and Mathematics of the Universe, University of Tokyo, Kashiwa, Chiba 277-8582, Japan*

(Received 6 January 2022; accepted 9 June 2022; published 27 June 2022)

The black hole singularity plays a crucial role in formulating Hawking's information paradox. The global spacetime analysis may be reconciled with unitarity by imposing a final state boundary condition on the spacelike singularity. Motivated by the final state proposal, we explore the effect of final state projection in two dimensional conformal field theories. We calculate the time evolution under postselection by employing the real part of pseudoentropy to estimate the amount of quantum entanglement averaged over histories between the initial and final states. We find that this quantity possesses a Page-curve-like behavior.

DOI: 10.1103/PhysRevD.105.126026

I. INTRODUCTION

The process of postselection is useful to study dynamical properties of quantum many-body systems and quantum field theories (QFTs). The nonunitary dynamics of projective measurements, for instance, provides a new tool for controlling many-body systems, giving rise to measurement-induced phase transitions [1,2]. Postselection also plays a key role in the black hole final state proposal [3], providing a possible resolution to the black hole information puzzle. Though the evaporation process due to Hawking radiation [4,5] might change the initial pure state into a mixed state [6], the final state remains pure under the state projection imposed on the spacelike singularity, cf. the left panel of Fig. 1. However, it has been pointed out that the final state has to be very special to preserve information [7]. Also a tension between the final state proposal and the presence of a smooth horizon was discussed in [8,9], for which a resolution was recently proposed in [10].

On the other hand, the unitarity in the black hole evaporating process requires that the amount of quantum entanglement between Hawking radiation and black hole interior follows the Page curve [11,12], based on the idea that the Bekenstein-Hawking entropy [5,13] gives the leading term for the logarithm of the number of black hole microstates.

It is essential to mention that studies of postselection in QFTs have been quite limited thus far. One reason for this may be the lack of universal and calculable quantities that can characterize the dynamical evolution of quantum states. For example, quantum quenches are often studied as a typical class of time-dependent systems, and entanglement entropy is important in probing how the systems thermalize [14].

However, in the presence of postselection, the use of entanglement entropy is limited—nevertheless, see [15–18]—since it only depends on a single state, namely either on the initial state or the final state. Instead, it is desirable to consider a universal quantity reflecting histories from the initial state $|\psi_i\rangle$ at time $t = 0$ to the final state $|\psi_f\rangle$ at $t = T$. It is important to note that at a specific time t we encounter two different quantum states $|\psi_1\rangle$ and $|\psi_2\rangle$, defined by

$$|\psi_1\rangle = e^{-iHt}|\psi_i\rangle, \qquad |\psi_2\rangle = e^{i(T-t)H}|\psi_f\rangle, \tag{1}$$

which are the evolution of the initial and final state till the time t, respectively. Recently, one such candidate, called pseudoentropy, has been introduced in [19]. Let us consider two pure states $|\psi_1\rangle$ and $|\psi_2\rangle$, and decompose the total system into the subsystems A and B such that the entire Hilbert space becomes factorized into $\mathcal{H}_{\text{tot}} = \mathcal{H}_A \otimes \mathcal{H}_B$. Taking the reduced transition matrix as

*ibrakal@yukawa.kyoto-u.ac.jp
†taishi.kawamoto@yukawa.kyoto-u.ac.jp
‡ruan.shanming@yukawa.kyoto-u.ac.jp
§takayana@yukawa.kyoto-u.ac.jp
‖zixia.wei@yukawa.kyoto-u.ac.jp

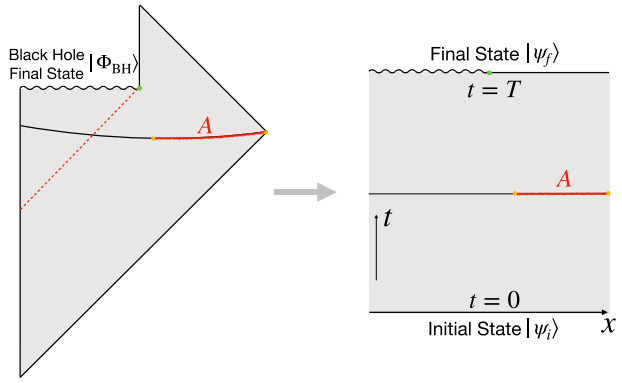

FIG. 1. Final state projection in an evaporating black hole (left) and its field theory simplification (right).

$$\tau_A^{1|2} = \mathrm{Tr}_B\left[\frac{|\psi_1\rangle\langle\psi_2|}{\langle\psi_2|\psi_1\rangle}\right], \tag{2}$$

the pseudoentropy is given by

$$S_A^{1|2} = -\mathrm{Tr}[\tau_A^{1|2}\log\tau_A^{1|2}]. \tag{3}$$

This quantity arises as a straightforward extension of holographic entanglement entropy [20,21] in the case of Euclidean time-dependent backgrounds [19]. Pseudoentropy is generically complex-valued as the transition matrix is not always Hermitian. However, we expect that the real part of pseudoentropy: $\mathrm{Re}[S_A^{1|2}]$, can be understood as the number of Bell pairs averaged over histories evolving from $|\psi_1\rangle$ to $|\psi_2\rangle$. Indeed, for a class of interesting quantum states, we can show explicitly that $\mathrm{Re}[S_A^{1|2}]$ coincides with the maximal number of Bell pairs distilled in our postselection process as found in [19] and more elaborated in Appendix A, stimulated by an old work [22]. Thus, this quantity is useful in figuring out quantum entanglement under postselection. Furthermore, it provides a nice quantum order parameter to distinguish different quantum phases [23,24]. Refer to [25–28] for further recent progress related to pseudoentropy.

The purpose of this article is to uncover the time evolution of pseudoentropy in conformal field theories (CFTs) under postselection, mainly motivated by the black hole final state proposal, as depicted in Fig. 1. An initial state $|\psi_i\rangle$ at time $t = 0$ evolves under the Hamiltonian H until $t = T$ when we perform the postselection to the final state $|\psi_f\rangle$. At time t, the initial state evolves into $|\psi_1\rangle = e^{-iHt}|\psi_i\rangle$, while the final state is reverted to $|\psi_2\rangle = e^{i(T-t)H}|\psi_f\rangle$. In this setup, sketched in the right panel of Fig. 1, we can define the pseudoentropy (3), which will be studied in this article. Note that if we apply the replica method by assuming a cut along the subsystem A, the familiar quantity given by $-\frac{\partial}{\partial n}\log\frac{Z_n}{(Z_1)^n}$, where Z_n is the partition function on the n-sheeted geometry, actually coincides with the pseudoentropy, but not with entanglement entropy for either $|\psi_1\rangle$ or $|\psi_2\rangle$. This quantity reduces to the entanglement entropy only when $|\psi_1\rangle = |\psi_2\rangle$.

Below, we often assume that our CFT has a classical gravity dual in order to obtain analytical results. Such a CFT, i.e., a so-called holographic CFT, is strongly coupled and has a large central charge c [29,30]. For this class of CFTs, we can evaluate correlation functions by employing the large c factorization such that they can be computed by Wick contractions.

II. HOMOGENEOUS POSTSELECTION AND GRAVITY DUAL

Consider the simplest model where we perform a postselection homogeneously. A tractable class of postselection can be defined by using the boundary state $|B\rangle$ (or Cardy state [31]) and considering the following two pure states in a given CFT

$$\begin{aligned}|\psi_1\rangle &= \mathcal{N}e^{-iHt}e^{-\delta H}|B\rangle,\\ |\psi_2\rangle &= \mathcal{N}e^{iH(T-t)}e^{-\delta H}|B\rangle,\end{aligned} \tag{4}$$

where the parameter δ denotes a UV regularization of the boundary state and $\mathcal{N}$ is the normalization factor. Note that $|\psi_1\rangle$ and $|\psi_2\rangle$ are obtained by evolving the initial and final state $|\psi_i\rangle = |\psi_f\rangle = \mathcal{N}e^{-\delta H}|B\rangle$ until the time t, following Eq. (1).

The inner product $\langle\psi_1|\psi_2\rangle$ defines a path-integral on the strip with the width $L = 2\delta + iT$. This is described as $0 \le \mathrm{Im}w \le L$ by taking $(w, \bar{w})$ as a complex coordinate. The conformal transformation, i.e., $z = e^{\frac{\pi w}{L}}$ maps this strip into an upper half-plane $\mathrm{Im}\, z > 0$. We set the two endpoints w_1, w_2 of the interval A as $(w_i, \bar{w}_i) = (x_i + i(\delta + it), x_i - i(\delta + it))$ with $i = 1, 2$. The n-sheeted partition function Z_n can be computed by inserting the twist operator σ_n at the two endpoints of A as in the usual field theory computation of entanglement entropy [32]. In holographic CFTs, this two-point function has two different saddle point contributions, namely, (i) the Wick contraction of two twist operators and (ii) the Wick contraction of each twist operator with their mirror images. Since the candidates of pseudoentropy computed from (i) and (ii) are dual to the length of the connected and disconnected geodesic, we write them as S_A^{con} and S_A^{dis}, respectively.

More generally, if we consider a conformal map from the original w coordinate to the upper half-plane in z coordinate via a holomorphic map $z = f(w)$, the two distinct contributions to pseudoentropy are given by

$$S_A^{\mathrm{con}} = \frac{c}{6}\log\frac{|f(w_1) - f(w_2)|^2}{\epsilon^2|f'(w_1)||f'(w_2)|}, \tag{5}$$

$$S_A^{\mathrm{dis}} = \frac{c}{6}\log\frac{|f(w_1) - \bar{f}(\bar{w}_1)||f(w_2) - \bar{f}(\bar{w}_2)|}{\epsilon^2|f'(w_1)||f'(w_2)|} + 2S_{\mathrm{bdy}}, \tag{6}$$

where S_{bdy} is referred to as the boundary entropy [33] and ϵ is a UV cutoff. This field-theoretic result perfectly agrees

with the holographic entanglement entropy in AdS/BCFT (anti-de Sitter/boundary CFT) [34–36].

Using the conformal map $z = e^{\frac{\pi w}{L}}$ for the present model, we obtain

$$S_A^{\rm con} = \frac{c}{3}\log\left[\frac{2T}{\pi\epsilon}\sin\left(\frac{\pi(x_2-x_1)}{2T}\right)\right],$$
$$S_A^{\rm dis} = \frac{c}{3}\log\left[\frac{2T}{\pi\epsilon}\sin\left(\frac{\pi t}{T}\right)\right] + i\frac{\pi c}{6} + 2S_{\rm bdy}, \qquad (7)$$

by taking the limit $\delta \to 0$. The correct pseudoentropy is given by the one with a smaller real part among the two. Note that $\mathrm{Re}[S_A^{\rm dis}]$ vanishes at $t = \epsilon/2$, which we regard as the initial time with a regularization. Then it increases logarithmically, reaching the maximum at the middle time $t = T/2$. It again decreases and vanishes at the final time $t = T - \epsilon/2$ as the boundary state does not have any real space entanglement [37]. However, $\mathrm{Re}[S_A^{\rm con}]$ is time-independent and is identical to the vacuum entanglement entropy. Taking the minimization, the disconnected contribution $\mathrm{Re}[S_A^{\rm dis}]$ dominates at early and late times. Depending on the value of $S_{\rm bdy}$, $\mathrm{Re}[S_A^{\rm con}]$ dominates for a finite period $t_* < t < T - t_*$.

The holographic analysis [38] based on AdS/BCFT suggests that a spacelike boundary in a Lorentzian BCFT has a complex-valued boundary entropy, namely

$$S_{\rm bdy} = \frac{c}{6}\log\sqrt{\frac{|\mathcal{T}|-1}{|\mathcal{T}|+1}} - i\frac{\pi c}{12}, \qquad (8)$$

where $\mathcal{T}$ is the tension of the end-of-the-world (EOW) brane dual to the boundary of the BCFT. This takes values in the range $\mathcal{T} < -1$. The imaginary part of (8) exactly cancels that of the pseudoentropy $S_A^{\rm dis}$.

For our setup (4), we can further construct its gravity dual as follows. Considering a global AdS_3, i.e.,

$$ds^2 = -\frac{T^2}{\pi^2}\cosh^2\rho dt^2 + d\rho^2 + \frac{T^2}{\pi^2}\sinh^2\rho dx^2, \qquad (9)$$

we introduce an EOW brane Q defined by

$$\cosh\rho\sin\frac{\pi t}{T} = \cosh\eta_0, \qquad (10)$$

that describes two-dimensional de Sitter spacetime. Here η_0 is related to the brane tension as $\mathcal{T} = -\coth\eta_0$. Finally, the gravity dual of the present CFT setup is given by the region surrounded by the AdS asymptotic boundary $\rho \to \infty$ and the EOW brane Q, as illustrated in Fig. 2. Similar to holographic entanglement entropy [20,21], the holographic pseudoentropy [19] is given by the geodesic length L_A in the corresponding Lorentzian gravity dual. In our case, due to the presence of Q, the geodesic connecting two endpoints of the interval A can end on Q, as shown in Fig. 2. Thus, we can have contributions from disconnected geodesics, denoted by $L_A^{\rm dis}$, in addition to those resulting from a connected geodesic $L_A^{\rm con}$. Accordingly, the real part of holographic pseudoentropy is taken to be the minimum as before,

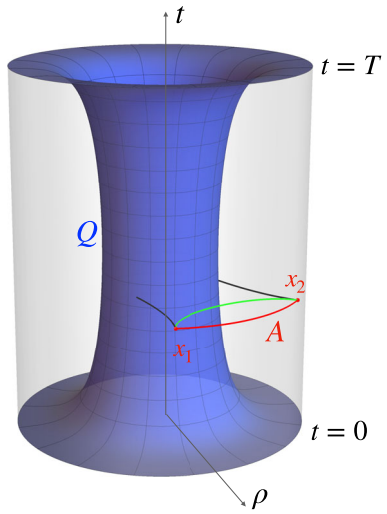

FIG. 2. The gravity dual of the Lorentzian BCFT. The blue surface describes the EOW brane defined in Eq. (10). For a subsystem A (red curve) located on the asymptotic boundary, the black and green curves denote the corresponding disconnected geodesics and the connected geodesic, respectively.

$$\mathrm{Re}[S_A^{1|2}] = \min\left[\mathrm{Re}\left[\frac{L_A^{\rm con}}{4G_{\rm N}}\right], \mathrm{Re}\left[\frac{L_A^{\rm dis}}{4G_{\rm N}}\right]\right]. \qquad (11)$$

Obviously, the connected contribution is the same as the holographic entanglement entropy in global AdS_3 and thus coincides with Eq. (5). Moreover, a straightforward computation for the sum of two geodesic lengths reproduces the disconnected contribution $S_A^{\rm dis}$. Thus, we can reproduce the CFT results from the gravity dual [39].

III. INHOMOGENEOUS POSTSELECTION AND PSEUDOENTROPY

Next, we focus on an example of inhomogeneous postselection models motivated by the black hole final state projection. Namely, at $t = 0$ we project the left part $x < 0$ and right part $x > 0$ to a boundary state $|B\rangle_{x<0}$ and the CFT vacuum $|0\rangle_{x>0}$ [40], respectively. This is realized by the (Euclidean) path-integral on the w-sheet as depicted in the left of Fig. 3. We regard the projection on $x < 0$ as the black hole final state [41]. Although the boundary state is based on a local boundary condition and does not have any real space entanglement [37], we expect that the time evolution $e^{i(T-t)H}$ may lead the state to a random chaotic one. We also qualitatively mimic the creation of entangled

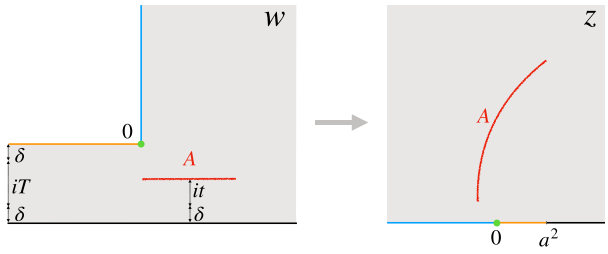

FIG. 3. A sketch of Euclidean path-integral on the w-sheet for inhomogeneous postselection and its conformal transformation to the upper half-plane in terms of the z coordinate. For $x < 0$, the path-integral is terminated at $\mathrm{Im}w = 0$ describing the projection to $|B\rangle_{x<0}$, while for $x > 0$ it extends to $\mathrm{Im}w = \infty$, corresponding to the projection to the vacuum state $|0\rangle_{x>0}$ on the right half.

pairs due to Hawking radiation during the time evolution of the initial boundary state as similar to quantum quenches [14].

Taking the initial state as the quantum quench state $e^{-\delta H}|B\rangle$, and fixing the final state as $e^{-\delta H}|B\rangle_{x<0} \otimes |0\rangle_{x>0}$, we can calculate the pseudoentropy from the general formulas (5) and (6). We choose the subsystem A as an interval between two points $(w_1, \bar{w}_1)$ and $(w_2, \bar{w}_2)$. More explicitly, one can find $(i = 1, 2)$

$$w_i = x_i + i(-\delta - i(T - t)),$$
$$\bar{w}_i = x_i - i(-\delta - i(T - t)). \tag{12}$$

We can also map the w-sheet to an upper half-plane (z-plane) via

$$w = \sqrt{z} - \frac{a}{2}\log\left[\frac{1+\frac{\sqrt{z}}{a}}{\frac{\sqrt{z}}{a}-1}\right] - \frac{a}{2}\pi i,$$
$$\bar{w} = \sqrt{\bar{z}} - \frac{a}{2}\log\left[\frac{1+\frac{\sqrt{\bar{z}}}{a}}{\frac{\sqrt{\bar{z}}}{a}-1}\right] + \frac{a}{2}\pi i, \tag{13}$$

by choosing $a = \frac{2}{\pi}(2\delta + iT)$.

For simplicity, we first examine the simple cases with $|x| \gg T$ to obtain some analytical results. We can evaluate the pseudoentropy in the following three regions: (a) $x_1, x_2 \gg T$, (b) $x_2 \gg T, x_1 \ll -T$, and (c) $x_1, x_2 \ll -T$ by setting $\delta = 0$ and noting that $t < T \ll |x_{1,2}|$.

In the case (a), $x_1, x_2 \gg T$, we obtain

$$\mathrm{Re}[S_A^{\mathrm{con}}] \simeq \frac{c}{6}\log\left[\frac{(x_1-x_2)^2(x_1+x_2)^2}{4x_1x_2\epsilon^2}\right],$$
$$\mathrm{Re}[S_A^{\mathrm{dis}}] \simeq \frac{c}{3}\log\left[\frac{2t}{\epsilon}\right] + 2\tilde{S}_{\mathrm{bdy}}, \tag{14}$$

where $\tilde{S}_{\mathrm{bdy}}$ is the real part of the boundary entropy S_{bdy} for spacelike surface. At $t = 0$, the disconnected one is favored and we have $\mathrm{Re}[S_A^{\mathrm{dis}}] = 0$. As time evolves, it grows logarithmically as $\mathrm{Re}[S_A^{\mathrm{dis}}] \simeq \frac{c}{3}\log\frac{2t}{\epsilon}$ and eventually $\mathrm{Re}[S_A^{\mathrm{con}}]$ becomes dominant. We can intuitively understand this phase transition behavior as follows. The state $|\psi_i\rangle = e^{-itH}e^{-\delta H}|B\rangle$ has quantum entanglement for the length scale $l < 2t$ due to causal propagation. Thus, if $|x_1 - x_2| < 2t$, both the initial state and final states have the corresponding quantum entanglement. However, if $|x_1 - x_2| > 2t$, the initial state does not have the entanglement at the length scale $|x_1 - x_2|$.

In the case (b), $x_2 \gg T$ and $x_1 \ll -T$, we obtain

$$\mathrm{Re}[S_A^{\mathrm{con}}] \simeq \frac{c}{6}\log\left[\frac{\pi^2 x_2^3}{32T\epsilon^2}\right],$$
$$\mathrm{Re}[S_A^{\mathrm{dis}}] \simeq \frac{c}{6}\log\left[\frac{4Tt\sin(\frac{\pi t}{T})}{\pi\epsilon^2}\right] + 2\tilde{S}_{\mathrm{bdy}}. \tag{15}$$

Since we assume $x_2 \gg T > t$, the disconnected one is favored at any time. It starts with $\mathrm{Re}[S_A^{\mathrm{dis}}] = 0$ as in the previous case and grows logarithmically as $\mathrm{Re}[S_A^{\mathrm{dis}}] \simeq \frac{c}{3}\log\frac{2t}{\epsilon}$ initially. Then it reaches a maximum and starts decreasing. At the final time $t \simeq T$, it is reduced to $\mathrm{Re}[S_A^{\mathrm{dis}}] \simeq \frac{c}{6}\log\frac{2T}{\epsilon}$. This result can be explained by noting that the entanglement in the part $x_1 < x < 0$ of region A becomes trivial at the final time due to postselection.

In the case (c), $x_1, x_2 \ll -T$, we simply reproduce our previous results (5) and (6). This can be easily understood if we note that for $x \ll -T$, the space looks like a strip having width T, identical to the homogeneous postselection model (4).

Next, we shall choose the subsystem to be $A = [0, y]$ with $y > 0$ to model the radiation subsystem for the evaporating black hole, where the black hole final state is imposed on $x < 0$ at $t = T$. We numerically plot the real part of pseudoentropy in Fig. 4. In particular, when we choose $y = \infty$, where only the disconnected geodesic is available, it looks like a Page curve, i.e., starting from $\mathrm{Re}[S_A] = 0$ and ending up with $\mathrm{Re}[S_A] = 0$. Indeed, since we have $w \simeq -\frac{z^{3/2}}{3a^2}$ when $z \simeq 0$, we can estimate the value at $t \simeq T$ as follows

$$\mathrm{Re}[S_A^{\mathrm{dis}}] \sim \frac{c}{12}\log\frac{|w|^2}{\epsilon^2} \simeq \frac{c}{6}\log\frac{(T-t)^2+\delta^2}{\epsilon^2}. \tag{16}$$

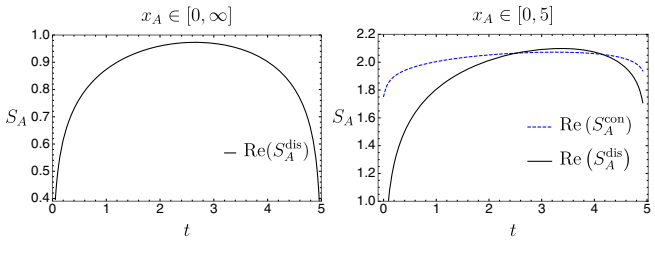

FIG. 4. The plot for the real part of pseudoentropy $\mathrm{Re}[S_A]$ for subsystems $A = [0, \infty]$ (left) and $A = [0, 5]$ (right) as a function of time t. We choose $T = 5$, $\delta = \epsilon = 0.01$ and $\tilde{S}_{\mathrm{bdy}} = 0$.

At $t = T$, this is of the same order as at the initial time $t = 0$. Therefore, we can conclude that the pseudoentropy vanishes at $t = T$ by choosing $\delta = O(\epsilon)$.

IV. PARTIAL POSTSELECTION AND PSEUDOENTROPY

Although the inhomogeneous postselection model studied before mimics a black hole spacetime with a spacelike singularity, there is a crucial difference with the black hole final state proposal [3]. In the latter, the postselection is only imposed on the singularity, while no operation is performed to the compliment part.

To model this feature, we shall consider partial postselection in a two-dimensional CFT, where we make a projection only for the left half $x < 0$. We again choose a global quench state $e^{-\delta H}|B\rangle$ at $t = 0$ as the initial state and consider its time evolution until the partial postselection is imposed at $t = T$. We take the postselected state as a boundary state $|B\rangle_{x<0}$, while keeping the right half $x > 0$ free. Therefore, right after the postselection at $t = T$, the quantum state associated with the whole system turns out to be

$$|B\rangle_{x<0} \otimes [\langle B|_{x<0}(e^{-iTH}e^{-\delta H}|B\rangle)]_{x>0} = (|B\rangle\langle B|_{x<0} \otimes I_{x>0}) \cdot e^{-iTH}e^{-\delta H}|B\rangle, \quad (17)$$

where $I_{x<0}$ is the identity matrix for the left half.

Next, we focus on the pseudoentropy at immediate time $0 < t < T$. In this case, the two pure states for evaluating the pseudoentropy are given by

$$|\psi_1\rangle = \mathcal{N}_1 e^{-itH}e^{-\delta H}|B\rangle,$$
$$|\psi_2\rangle = \mathcal{N}_2 e^{-i(t-T)H}(|B\rangle\langle B|_{x<0} \otimes I_{x>0}) \cdot e^{-iTH}e^{-\delta H}|B\rangle, \quad (18)$$

where $\mathcal{N}_{1,2}$ are normalization factors. Taking subsystem A to be an interval, the pseudoentropy (3) in this setup can be computed via the Euclidean path-integral shown in the left panel of Fig. 5. Using the conformal map

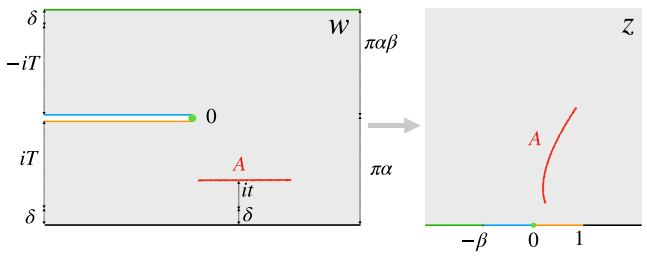

FIG. 5. A sketch of the path-integral description of partial postselection (left) and its conformal map to the upper half-plane (right).

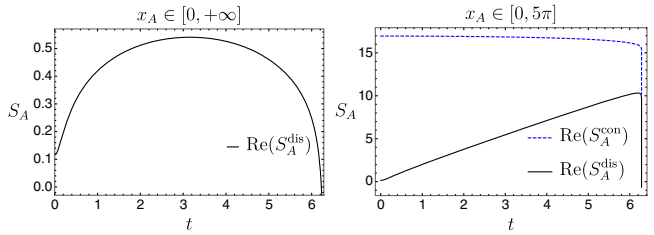

FIG. 6. The plot for the real part of pseudoentropy $\mathrm{Re}[S_A]$ for subsystems $A = [0, \infty]$ (left) and $A = [0, 5\pi]$ (right) as a function of time t. We choose the parameters $T = 2\pi$, $\delta = \varepsilon = 0.05\pi$.

$$w(z) = f^{-1}(z) = \alpha \log(1 - z) + \alpha\beta \log\left(\frac{z + \beta}{\beta}\right), \quad (19)$$

we can map the strip geometry with a slit to the upper half-plane as shown in the right of Fig. 5. The parameters α and β are fixed by $\pi\alpha = \delta + iT$ and $\pi\alpha\beta = \delta - iT$, respectively. For the subsystem $A = [0, y]$, with $y > 0$, we plot the real part of pseudoentropy in Fig. 6. This again shows a Page-curve-like behavior.

V. DISCUSSION

We have studied the time evolution of pseudoentropy under postselection, whose real part provides an estimation of the amount of quantum entanglement, i.e., the number of Bell pairs averaged over histories between the initial state and the postselected final state. In a two-dimensional CFT setup, where postselection applies to the left region, $x < 0$, the mentioned entanglement measure associated with the region $x > 0$ possesses a Page-curve-like behavior. It grows by starting from zero, reaches its maximum, decreases, and eventually vanishes at the time of the partial postselection. Our setups model black hole evaporation according to the final state projection scenario.

Note that we have obtained the Page curve result for the radiation entanglement by employing the notion of pseudoentropy. However, postselection is not captured by entanglement entropy obtained from the reduced density matrix of a single pure state. This shows the usefulness of pseudoentropy as a measure of quantum entanglement under postselection. At the same time, this motivates us to compare the final state proposal with the island picture [42–44], which also leads to the Page curve. Notably, in our analysis, the unitarity-caused deviation from monotonical increase arises due to the past evolution of the postselected final state. This qualitatively looks similar to the island scenario suggesting a modification of the Hilbert space structure inside the black hole. However, state projection seems to affect correlations already in the initial stages of evaporation. There is no sudden appearance of a disjoint entanglement region on a Cauchy slice residing in the interior right after the Page time.

Considerations that seem to indicate a tension between the final state proposal and the presence of a smooth

horizon have been discussed in [8,9], where a resolution to the puzzle raised in [9] has been proposed in [10]. Nevertheless, starting from the arguments in [45], we shall emphasize that indications of a drama for infalling observers are merely an artifact of the factorizable Hilbert space within the improper semiclassical treatment. On the other hand, the notion of a classical singularity may already have to be given up when the black hole is young, following the arguments by Page [46]. This motivates considering sequential projective measurements scanning through a smeared interior patch. It might be possible that associated correlations responsible for the Page curve make it to the exterior near-horizon region, namely in a nontrivially protected form [47]. A correct treatment of the singularity might thus have imprints not only behind the horizon. We want to return to some of these aspects in the near future. Another interesting direction is studying state projection in moving mirrors [48] by employing their holographic formulation [49,50].

ACKNOWLEDGMENTS

We are grateful to Tokiro Numasawa and Kotaro Tamaoka for useful discussions and especially to Ahmed Almheiri and Andrew Strominger for valuable comments on a draft of this paper. We would also like to thank the YITP workshop: KIAS-YITP 2021: String Theory and Quantum Gravity (YITP-W-21-18), hosted by YITP, Kyoto University, for stimulating discussions and comments from participants, where this work was presented by T. K. This work is supported by MEXT-JSPS Grant-in-Aid for Transformative Research Areas (A) "Extreme Universe", No. 21H05187. T. T. is also supported by JSPS Grant-in-Aid for Scientific Research (A) No. 21H04469. S.-M. R. and T. T. are supported by the Simons Foundation through the "It from Qubit" collaboration. T. T. is also supported by Inamori Research Institute for Science and World Premier International Research Center Initiative (WPI Initiative) from MEXT. Z. W. is supported by Grant-in-Aid for JSPS Fellows No. 20J23116.

APPENDIX A: PSEUDOENTROPY AND POSTSELECTION

In the following, we present an argument suggesting that the real part of pseudoentropy can measure quantum entanglement when we take an average over the evolution from the initial state to the final state under postselection.

Let us consider the decoherence function [22] for the projective measurement $\sum_k \Pi_k = 1$ defined by

$$D_{k,l} = \frac{1}{\mathrm{Tr}[\rho_1\rho_2]}\mathrm{Tr}[\rho_2\Pi_k\rho_1\Pi_l], \tag{A1}$$

where ρ_1 and ρ_2 denote the initial and final density matrix, respectively. This quantity measures the inference of probability of k-event and l-event. When the decoherence function is diagonal, the histories completely decohere. If we set $\rho_2 = I$, the above quantity is reduced to the ordinary probability distribution

$$D_{k,l} = \mathrm{Tr}[\Pi_k\rho_i\Pi_l]. \tag{A2}$$

When both the initial and final state are pure, we have

$$D_{k,l} = \frac{\langle\psi_f|\Pi_k|\psi_i\rangle\langle\psi_i|\Pi_l|\psi_f\rangle}{|\langle\psi_f|\psi_i\rangle|^2}. \tag{A3}$$

As in [19], let us consider two-qubit states $|\psi_1\rangle$ and $|\psi_2\rangle$ of the following form

$$\begin{aligned}|\psi_1\rangle &= c_1|00\rangle_{AB} + s_1|11\rangle_{AB},\\ |\psi_2\rangle &= c_2|00\rangle_{AB} + s_2|11\rangle_{AB},\end{aligned} \tag{A4}$$

where $c_{1,2}$ and $s_{1,2}$ can take any complex values with the constraints $|c_1|^2+|s_1|^2=1$ and $|c_2|^2+|s_2|^2=1$ imposed. To have a better counting of Bell pairs, we take the asymptotic limit $M\to\infty$, by considering M copies of the original states: $|\psi_i\rangle = (|\psi_1\rangle)^{\otimes M}$ and $|\psi_f\rangle = (|\psi_2\rangle)^{\otimes M}$. The total Hilbert space now consists of $2M$ qubits, i.e., M copies of the A spin and M copies of the B spin. We call the former $\tilde{A}$ and the latter $\tilde{B}$. We choose Π_k to be the projection which acts only on the M spins in $\tilde{A}$ such that the states with k up spins (i.e., $|1\rangle$) and $M-k$ down spins (i.e., $|0\rangle$) for M-qubit states are selected. Π_k acts on $\tilde{B}$ as an identity. After the projection by Π_k, we obtain a state with maximal entanglement between $\tilde{A}$ and $\tilde{B}$. Due to this projection there remain ${}_MC_k \equiv \frac{M!}{k!(M-k)!}$ states. This is the same procedure as in [19], where an operational interpretation of pseudoentropy was presented for this special class of states.

We naturally define the averaged value $\bar{N}$ of Bell pairs when we fix both the initial and final state in the asymptotic limit as follows

$$\bar{N} = \lim_{M\to\infty}\frac{N_{\max}}{M}, \tag{A5}$$

where

$$N_{\max} = \sum_{k,l} D_{k,l}\left(\frac{\log({}_MC_k) + \log({}_MC_l)}{2}\right). \tag{A6}$$

Here, $N_{\max}$ estimates the maximal number of Bell pairs, which can be distilled by local operation and classical communication (LOCC) in the asymptotic limit $M\to\infty$ when we take the average over histories from the initial state to the final state. We can explicitly write

$$D_{k,l} = p_k p_l^*, \tag{A7}$$

with

$$p_k = \frac{\langle\psi_f|\Pi_k|\psi_i\rangle}{\langle\psi_f|\psi_i\rangle}. \tag{A8}$$

Note that p_k take complex values in general since we allow $c_{1,2}$ and $s_{1,2}$ to take complex values. Due to the identity $\sum_k p_k = 1$, we can rewrite $N_{\max}$ as

$$N_{\max} = \mathrm{Re}\left[\sum_k p_k \log({}_M C_k)\right]. \tag{A9}$$

As shown in [19], the quantity $\sum_k p_k \log({}_M C_k)$ coincides with the pseudoentropy (3) in the limit $M \to \infty$. Therefore, it implies that the real part of pseudoentropy can be interpreted as the number of distillable Bell pairs averaged over the history between the initial state and final state. In this argument, we have assumed the specific class of initial and final states given by (A4). They share the same basis of spins, i.e., $|00\rangle_{AB}$ and $|11\rangle_{AB}$, and we can easily fix the form of the projection Π_k. To extend this analysis to general states, we need to pick up an appropriate projection Π_k to extract Bell pairs, which is not obvious for generic choices of $|\psi_1\rangle$ and $|\psi_2\rangle$. We will leave this general argument to future work.

APPENDIX B: ANALYSIS OF END-OF-THE-WORLD BRANES IN AdS_3

We focus on the end-of-the-world (EOW) brane in global AdS_3 (9) defined by (10). This surface is described by its world-sheet coordinates (τ, x) introduced as follows

$$\begin{aligned}
X_0 &= \cosh\rho\,\cos\frac{\pi t}{T} = \sinh\tau\,\sinh\eta_0,\\
X_1 &= \sinh\rho\,\sin\frac{\pi x}{T} = \cosh\tau\,\sinh\eta_0\,\sin\frac{\pi x}{T},\\
X_2 &= \sinh\rho\,\cos\frac{\pi x}{T} = \cosh\tau\,\sinh\eta_0\,\cos\frac{\pi x}{T},\\
X_3 &= \cosh\rho\,\sin\frac{\pi t}{T} = \cosh\eta_0,
\end{aligned} \tag{B1}$$

where the original AdS_3 defined by $X_0^2+X_3^2=X_1^2+X_2^2+1$ in the spacetime with line element $ds^2 = -(dX_0)^2 - (dX_3)^2 + (dX_1)^2 + (dX_2)^2$. The induced metric of the brane Q is derived as

$$ds^2|_Q = \sinh^2\eta_0\left(-d\tau^2 + \frac{\pi^2}{T^2}\cosh^2\tau dx^2\right), \tag{B2}$$

which is nothing but a two-dimensional de Sitter space.

To evaluate the geodesic length, it is useful to rewrite the global AdS_3 in terms of Poincaré coordinates, i.e.,

$$\begin{aligned}
X_0 &= \frac{1+z_{\mathrm{P}}^2+x_{\mathrm{P}}^2-t_{\mathrm{P}}^2}{2z_{\mathrm{P}}},\\
X_3 &= \frac{t_{\mathrm{P}}}{z_{\mathrm{P}}},\\
X_1 &= \frac{x_{\mathrm{P}}}{z_{\mathrm{P}}},\\
X_2 &= \frac{1-z_{\mathrm{P}}^2-x_{\mathrm{P}}^2+t_{\mathrm{P}}^2}{2z_{\mathrm{P}}},
\end{aligned} \tag{B3}$$

with the metric $ds^2 = \frac{dz_{\mathrm{P}}^2 - dt_{\mathrm{P}}^2 + dx_{\mathrm{P}}^2}{z_{\mathrm{P}}^2}$. The surface Q mapped to the plane is thus located at

$$\frac{t_{\mathrm{P}}}{z_{\mathrm{P}}} = \cosh\eta_0. \tag{B4}$$

It is also useful to note that we have $x_{\mathrm{P}} = \frac{\sin\frac{\pi x}{T}}{\cos\frac{\pi t}{T}+\cos\frac{\pi x}{T}}$ and $t_{\mathrm{P}} = \frac{\sin\frac{\pi t}{T}}{\cos\frac{\pi t}{T}+\cos\frac{\pi x}{T}}$ at the AdS boundary.

In Poincaré coordinates, the geodesic length between a boundary point at t_{P} and the surface Q is given by $\log\left[\frac{2t_{\mathrm{P}}}{\epsilon}e^{-\eta_0}\right]$ (refer to e.g., [38]). As a result, we can reproduce Eq. (7). The condition that the connected geodesic connecting two boundary points $(t_{\mathrm{P}}, x_{\mathrm{P}}^{(1)})$ and $(t_{\mathrm{P}}, x_{\mathrm{P}}^{(2)})$ does not touch the surface Q is given by

$$|x_{\mathrm{P}}^{(2)} - x_{\mathrm{P}}^{(1)}| < 2z_{\mathrm{P}}^*, \tag{B5}$$

where z_{P}^* denotes the value of z_{P} at the time t_{P} on the surface Q, i.e., $z_{\mathrm{P}}^* = \frac{t_{\mathrm{P}}}{\cosh\eta_0}$.

Now let us choose two arbitrary boundary points in Poincaré coordinates. A half of their connected geodesic is parametrized by

$$\begin{aligned}
z_{\mathrm{p}}(s) &= z_{\max}\,\sin(s),\\
t_{\mathrm{p}}(s) &= t_{\mathrm{P}}^{(1)} + \frac{\Delta t_{\mathrm{P}}}{\sqrt{\Delta x_{\mathrm{P}}^2 - \Delta t_{\mathrm{P}}^2}} z_{\max}(1-\cos(s))\\
&= t_{\mathrm{P}}^{(1)} + \Delta t_{\mathrm{P}}\sin^2\left(\frac{s}{2}\right),
\end{aligned} \tag{B6}$$

where we have defined

$$\Delta x_{\mathrm{P}} = x_{\mathrm{P}}^{(2)} - x_{\mathrm{P}}^{(1)}, \quad \Delta t_{\mathrm{P}} = t_{\mathrm{P}}^{(2)} - t_{\mathrm{P}}^{(1)}, \quad z_{\max} = \frac{\sqrt{\Delta x_{\mathrm{P}}^2 - \Delta t_{\mathrm{P}}^2}}{2}. \tag{B7}$$

If the connected geodesic does not touch the brane Q, we arrive at the following condition, i.e.,

$$z_{\mathrm{P}}^*(t_{\mathrm{P}}(s)) \geq z_{\mathrm{p}}(s). \tag{B8}$$

Substituting the geodesic solutions, one can get

$$\left(t_{\mathrm{P}}^{(1)}+\Delta t_{\mathrm{P}}\sin^2\left(\frac{s}{2}\right)\right)\frac{1}{\sin(s)}\geq z_{\max}\cosh\eta_0, \tag{B9}$$

which should hold along the whole geodesic. It is straightforward to find the minimum of the left-hand side of the above inequality is achieved by taking

$$\tan(s^*)=\frac{2\sqrt{t_{\mathrm{P}}^{(2)}t_{\mathrm{P}}^{(1)}}}{t_{\mathrm{P}}^{(2)}-t_{\mathrm{P}}^{(1)}}. \tag{B10}$$

Correspondingly, the inequality is finally given by

$$2\sqrt{t_{\mathrm{P}}^{(2)}t_{\mathrm{P}}^{(1)}}\geq\sqrt{\Delta x_{\mathrm{P}}^2-\Delta t_{\mathrm{P}}^2}\cosh\eta_0. \tag{B11}$$

Of course, it simply reduces to the condition Eq. (B5) by taking $t_{\mathrm{P}}^{(1)}=t_{\mathrm{P}}^{(2)}$. For our interested case with two boundary points on the same time slice in global coordinate, we can find that the corresponding boundary points are located at different Poincaré coordinate times, i.e.,

$$x_{\mathrm{P}}^{(i)}=\frac{\sin\frac{\pi x_i}{T}}{\cos\frac{\pi t}{T}+\cos\frac{\pi x_i}{T}},\qquad t_{\mathrm{P}}^{(i)}=\frac{\sin\frac{\pi t}{T}}{\cos\frac{\pi t}{T}+\cos\frac{\pi x_i}{T}}. \tag{B12}$$

The connected contribution arises only when the connected geodesic does not touch the EOW brane Q, which leads to the following condition

$$\sin\frac{\pi t}{T}>\cosh\eta_0\cdot\sin\frac{\pi(x_2-x_1)}{2T}. \tag{B13}$$

It is easy to find that it is the same condition shown in Eq. (B11) with using Eq. (B12).

[1] B. Skinner, J. Ruhman, and A. Nahum, Measurement-Induced Phase Transitions in the Dynamics of Entanglement, Phys. Rev. X **9**, 031009 (2019).
[2] Y. Li, X. Chen, and M. P. A. Fisher, Quantum Zeno effect and the many-body entanglement transition, Phys. Rev. B **98**, 205136 (2018).
[3] G. T. Horowitz and J. M. Maldacena, The black hole final state, J. High Energy Phys. 02 (2004) 008.
[4] S. W. Hawking, Black hole explosions, Nature (London) **248**, 30 (1974).
[5] S. W. Hawking, Particle creation by black holes, Commun. Math. Phys. **43**, 199 (1975); Erratum, Commun. Math. Phys. **46**, 206 (1976).
[6] S. W. Hawking, Breakdown of predictability in gravitational collapse, Phys. Rev. D **14**, 2460 (1976).
[7] D. Gottesman and J. Preskill, Comment on "The black hole final state", J. High Energy Phys. 03 (2004) 026.
[8] S. Lloyd and J. Preskill, Unitarity of black hole evaporation in final-state projection models, J. High Energy Phys. 08 (2014) 126.
[9] R. Bousso and D. Stanford, Measurements without probabilities in the final state proposal, Phys. Rev. D **89**, 044038 (2014).
[10] Talk by A. Almheiri, Comments on the black hole final state proposal and the gravitational path integral, at YITP workshop "Recent progress in theoretical physics based on quantum information theory", 2021, http://www2.yukawa.kyoto-u.ac.jp/qith2021/Almheiri.pdf.
[11] D. N. Page, Average Entropy of a Subsystem, Phys. Rev. Lett. **71**, 1291 (1993).
[12] D. N. Page, Information in Black Hole Radiation, Phys. Rev. Lett. **71**, 3743 (1993).
[13] J. D. Bekenstein, Black holes and entropy, Phys. Rev. D **7**, 2333 (1973).
[14] P. Calabrese and J. L. Cardy, Evolution of entanglement entropy in one-dimensional systems, J. Stat. Mech. (2005) P04010.
[15] M. A. Rajabpour, Post measurement bipartite entanglement entropy in conformal field theories, Phys. Rev. B **92**, 075108 (2015).
[16] M. Rajabpour, Fate of the area-law after partial measurement in quantum field theories, arXiv:1503.07771.
[17] M. A. Rajabpour, Entanglement entropy after a partial projective measurement in $1+1$ dimensional conformal field theories: Exact results, J. Stat. Mech. (2016) 063109.
[18] T. Numasawa, N. Shiba, T. Takayanagi, and K. Watanabe, EPR pairs, local projections and quantum teleportation in holography, J. High Energy Phys. 08 (2016) 077.
[19] Y. Nakata, T. Takayanagi, Y. Taki, K. Tamaoka, and Z. Wei, New holographic generalization of entanglement entropy, Phys. Rev. D **103**, 026005 (2021).
[20] S. Ryu and T. Takayanagi, Holographic Derivation of Entanglement Entropy from AdS/CFT, Phys. Rev. Lett. **96**, 181602 (2006).
[21] V. E. Hubeny, M. Rangamani, and T. Takayanagi, A covariant holographic entanglement entropy proposal, J. High Energy Phys. 07 (**2007**) 062.
[22] M. Gell-Mann and J. B. Hartle, Quantum mechanics in the light of quantum cosmology, arXiv:1803.04605.
[23] A. Mollabashi, N. Shiba, T. Takayanagi, K. Tamaoka, and Z. Wei, Pseudo Entropy in Free Quantum Field Theories, Phys. Rev. Lett. **126**, 081601 (2021).
[24] A. Mollabashi, N. Shiba, T. Takayanagi, K. Tamaoka, and Z. Wei, Aspects of pseudoentropy in field theories, Phys. Rev. Research **3**, 033254 (2021).
[25] G. Camilo and A. Prudenziati, Twist operators and pseudo entropies in two-dimensional momentum space, arXiv:2101.02093.

[26] T. Nishioka, T. Takayanagi, and Y. Taki, Topological pseudo entropy, J. High Energy Phys. 09 (2021) 015.
[27] K. Goto, M. Nozaki, and K. Tamaoka, Subregion spectrum form factor via pseudo entropy, Phys. Rev. D **104**, L121902 (2021).
[28] M. Miyaji, Island for gravitationally prepared state and pseudo entanglement wedge, J. High Energy Phys. 12 (2021) 013.
[29] I. Heemskerk, J. Penedones, J. Polchinski, and J. Sully, Holography from conformal field theory, J. High Energy Phys. 10 (2009) 079.
[30] T. Hartman, C. A. Keller, and B. Stoica, Universal spectrum of 2d conformal field theory in the large c limit, J. High Energy Phys. 09 (2014) 118.
[31] J. L. Cardy, Boundary conditions, fusion rules and the Verlinde formula, Nucl. Phys. **B324**, 581 (1989).
[32] P. Calabrese and J. L. Cardy, Entanglement entropy and quantum field theory, J. Stat. Mech. (2004) P06002.
[33] I. Affleck and A. W. W. Ludwig, Universal Noninteger "Ground State Degeneracy" in Critical Quantum Systems, Phys. Rev. Lett. **67**, 161 (1991).
[34] T. Takayanagi, Holographic Dual of BCFT, Phys. Rev. Lett. **107**, 101602 (2011).
[35] M. Fujita, T. Takayanagi, and E. Tonni, Aspects of AdS/BCFT, J. High Energy Phys. 11 (2011) 043.
[36] A. Karch and L. Randall, Open and closed string interpretation of SUSY CFT's on branes with boundaries, J. High Energy Phys. 06 (**2001**) 063.
[37] M. Miyaji, S. Ryu, T. Takayanagi, and X. Wen, Boundary states as holographic duals of trivial spacetimes, J. High Energy Phys. 05 (2015) 152.
[38] I. Akal, Y. Kusuki, T. Takayanagi, and Z. Wei, Codimension two holography for wedges, Phys. Rev. D **102**, 126007 (2020).
[39] See Appendix B for more details.
[40] Here the vacuum state (or ground state) $|0\rangle_{x>0}$ is defined on the semi-infinite line $x > 0$ and constructed by a path integral with infinite Euclidean time evolution. For example, in our setup of the left panel of Fig. 3, if we insert two operators at the boundary of the subsystem A, the full path-integral computes to $\langle B|_{x<0}\langle 0|_{x>0}e^{-\delta H}O(x_1)O(x_2)e^{-(\delta+iT)H}|0\rangle_{-\infty<x<\infty}$.
[41] One may wonder whether the boundary state $|B\rangle$ imposed on $x < 0$ can mimic the black hole final state since the latter is expected to be very random [3]. However, it is worth emphasizing that, as commented in [7], the state which is expected to be random should be a time-reverted state of the black hole final state, but not itself. Therefore, there is no apparent contradiction that a boundary state can mimic the black hole final state.
[42] G. Penington, Entanglement wedge reconstruction and the information paradox, J. High Energy Phys. 09 (2020) 002.
[43] A. Almheiri, N. Engelhardt, D. Marolf, and H. Maxfield, The entropy of bulk quantum fields and the entanglement wedge of an evaporating black hole, J. High Energy Phys. 12 (2019) 063.
[44] A. Almheiri, R. Mahajan, J. Maldacena, and Y. Zhao, The page curve of Hawking radiation from semiclassical geometry, J. High Energy Phys. 03 (2020) 149.
[45] A. Almheiri, D. Marolf, J. Polchinski, and J. Sully, Black holes: Complementarity or Firewalls?, J. High Energy Phys. 02 (2013) 062.
[46] I. Akal, Information storage and near horizon quantum correlations, arXiv:2109.01639.
[47] I. Akal, Universality, intertwiners and black hole information, arXiv:2010.12565.
[48] I. Akal, T. Kawamoto, S.-M. Ruan, T. Takayanagi, and Z. Wei, Zoo of holographic moving mirrors, arXiv:2205.02663.
[49] I. Akal, Y. Kusuki, N. Shiba, T. Takayanagi, and Z. Wei, Entanglement Entropy in a Holographic Moving Mirror and the Page Curve, Phys. Rev. Lett. **126**, 061604 (2021).
[50] I. Akal, Y. Kusuki, N. Shiba, T. Takayanagi, and Z. Wei, Holographic moving mirrors, Classical Quantum Gravity **38**, 224001 (2021).